JOURNAL OF MATERIALS SCIENCE **35** (2000) 5751–5765

The use of digital images to determine deformation throughout a microstructure

Part II *Application to cement paste*

C. M. NEUBAUER*,§, H. M. JENNINGS*,‡
*Departments of *Materials Science and ‡Civil Engineering, Northwestern University, Evanston, IL 60208, USA*
E-mail: h-jennings@nwu.edu

The deformation mapping technique (DMT) was applied to the problem of studying shrinkage in cement paste during drying. The results are used to help refine our understanding of the mechanisms that cause shrinkage for different relative humidity ranges. The influences of the age, water : cement ratio, and curing temperature on drying shrinkage are examined. In all cases, shrinkage of bulk samples results from the interaction between expanding regions (rarefactions) and contracting regions (compactions) within the microstructure. Very large local deformations are associated with the collapse of the colloid networks of C-S-H. Damage, akin to fracture, is observed in stiffer samples.

1. Introduction

The deformation mapping technique (DMT) utilized in this study has been described and validated in Part I [1]. This paper is aimed at applying the technique to cement paste.

Microstructure takes on meaning at many levels in materials science. It usually focuses on the size, shape, and distribution of phases within a material. There is, however, no reason why mapping deformation in the microstructure could not equally be a description of the deformation of regions that are subjected to stress within a material. This is particularly important for heterogeneous materials such as cement paste.

Stress-induced deformations within the microstructure in cement paste are only beginning to be quantitatively investigated. These stresses can have many sources, including chemical, environmental, thermal, or mechanical. An important type of stress in hardened concrete comes from drying. Since water is an integral part of the cement paste matrix, changes in relative humidity result in drying stresses and overall shrinkage. Drying shrinkage is complicated, consisting of both reversible (elastic) and irreversible (viscoelastic) components.

An additional complication is the notion of both intrinsic (restraint free, sometimes referred to as real [2]) shrinkage and extrinsic (bulk, sometimes referred to as apparent [2]) shrinkage. Intrinsic mechanisms are associated with the material properties of cement paste and are independent of specimen geometry. Extrinsic mechanisms are dependent upon specimen geometry; for example, the thickness of a sample may result in a moisture gradient across a specimen causing differential shrinkage and possibly cracking. Thus, in order to study intrinsic mechanisms, very small specimens, on the scale of millimeters or less, and/or very slow drying must be employed to avoid moisture gradients.

The only known direct observations at the micrometer scale of a cement paste during drying is in the work of Bergstrom [3] (also presented in Neubauer *et al*. [4]). In these studies, an environmental scanning electron microscope (ESEM) was used to study the drying shrinkage of cement paste as a function of water/cement (w/c) ratio, age, curing temperature, and drying rate. A series of images at different relative humidities (RH) was analyzed using an image intensity matching technique (IIMT) that calculated displacements throughout the microstructure relative to a given reference point [5]. This allowed the average drying shrinkage strain to be estimated by examining several sets of points in the images and computing the drying-induced change across the distance between pairs of points. While these results provide an estimate of the magnitude of the total average deformation, no information about the distribution of deformations within the microstructure was presented. Because areas of localized deformation are the ultimate cause of failure, the distribution of deformations is often more important than the macro-scale deformation.

It is important to note that the term deformation is used, instead of strain, as there are certainly viscoelastic effects and possibly localized debonding in drying shrinkage. *Deformation* means local displacement or, in the case of this paper, change in the local area of some recognizable feature, whether elastically recoverable or not. Positive deformations (areas which expand)

§ *Present Address*: Valspar Corporation, Global Packaging Center, Pittsburgh, PA 15233, USA.

are termed *rarefactions* and negative deformations (areas which shrink) are termed *compactions*. Although strain may be technically correct, we use deformation so that there is no ambiguity.

The relative importance of the various shrinkage mechanisms in cement paste [6] at different RH values is still the subject of debate. The authors acknowledge that to quantitatively sort out the influence of the various mechanisms at different RH values, the type of result obtained from DMT must be coupled with careful three dimensional models that include rate of drying, creep, pore size and distribution of pore size, and other variables. This is beyond the scope of this research; however, qualitative insight can be gained from DMT results as will be demonstrated below.

1.1. Drying shrinkage mechanisms

Roper [7] examined shrinkage vs. weight loss in small bars of cement paste approximately 6 mm × 6 mm × 127 mm, using two w/c ratios, 0.35 and 0.5. Samples were carefully equilibrated to various relative humidities so that his results can be interpreted in terms of intrinsic and not extrinsic (i.e. size-related) drying shrinkage mechanisms. He found that when shrinkage was graphed vs. weight loss, there were four linear regions, and three points where the slope changed abruptly at approximately 85%, 40% and 25% RH. From this he deduced that there were four basic mechanisms of shrinkage which have been widely referred to since. The four [8–11] most important and widely accepted [12] are: (1) capillary stress, (2) disjoining pressure, (3) Gibbs-Bangham shrinkage, and (4) the removal of interlayer water. These mechanisms are summarized in Table I.

Capillary stress is a mechanism that operates at high relative humidities as the capillary pores empty. The stresses are the result of menisci that form as liquid evaporates and empties the pore [12–17]. The tension in the menisci is transferred to the pore walls, causing contraction of the solid frame and resulting in shrinkage. This mechanism is important down to about 50% RH and when, presumably, the larger gel pores are emptying. It should be noted that the distinction between gel pores and capillary pores is vague, as the pore size distribution varies continuously within the size range that would separate gel and capillary pores.

Disjoining pressure also operates at high relative humidity [7, 12–15, 18, 19]. When a relatively thick layer of water is adsorbed on the surfaces of calcium silicate hydrate (C-S-H) particles, the resulting repulsive force between C-S-H particles is greater than the Van der Waal's forces drawing the particles together. This forces the particles apart with a wedge of adsorbed water [12]. As the relative humidity is lowered, adsorbed water is removed via the wide side of the wedge, causing the adsorbed layers to become thinner.

Gibbs-Bangham shrinkage operates at lower relative humidities [2, 12–17, 20]. Adsorbed water molecules on the C-S-H surfaces desorb, resulting in unsatisfied surface bonds on the C-S-H particles. This causes the surface free energy to increase, which in turn causes particles to attract and paste to shrink.

The final mechanism, *removal of interlayer water*, operates only at very low relative humidities (< 11% RH) [12–17]. Feldman and Sereda [21] have speculated that this mechanism may cause layers to collapse as water is removed. They also hypothesized that bonds are formed between layers, which results in irreversible shrinkage.

Part of the present study has been designed to be able to compare our results with Roper's work. In addition, to examine basic mechanisms, the effects of water : cement ratio and curing temperature on drying shrinkage are described.

TABLE I Summary of drying shrinkage mechanisms occurring in cement paste

Mechanism	Relative Humidity Range	Important Phases
Capillary Stresses	40–90%	Capillary porosity
Disjoining Pressure	50–90%	C-S-H
Gibbs-Bangham Shrinkage	<30%	C-S-H
Removal of Interlayer Water	<11%	C-S-H

2. Experimental

Samples were prepared by hand mixing cement with deionized water for 5 minutes, placing them on a rolling mill overnight to prevent sedimentation prior to hardening, and then storing them in lime water baths at the appropriate temperature until testing age. The influence of w/c, age, and curing temperature are explored using the variables outlined in Table II.

Once a sample reached the desired age, it was removed from the water bath and broken apart using a hammer. Several flakes approximately 1 cm^2 × 1 mm were collected and placed in the specimen chamber of the environmental scanning electron microscope (ESEM) at the initial relative humidity (90% RH) and allowed to equilibrate for approximately 30 minutes. It was determined that 30 minutes was more than sufficient a period of time for deformation to occur and the sample to stabilize (10–15 minutes was actually adequate). Images of selected areas were taken. Then the relative humidity in the chamber was dropped to the next lower level and again allowed to equilibrate for approximately 30 minutes before new images of the selected areas were acquired. This process was repeated for all of the desired relative humidities.

To relate our results to those of Roper [7], two cement paste samples, with $w/c = 0.35$ and $w/c = 0.50$ were aged for 7 days at room temperature. Images were collected at 90%, 80%, 75%, 55%, 35%, 25%, and 20% RH. Using the 90% RH image as the reference undeformed image, deformation maps and distributions were produced at each lower RH value, using the deformation mapping technique (DMT) described in

TABLE II Cement paste samples used in the present study: w/c ratio, curing ages, and curing temperatures

w/c	Age (days)	Curing Temperature (°C)
0.3	4, 14, 28	20, 30, 40
0.4	4, 14, 28	20
0.5	4, 14, 28	20

Part I [1]. The temperature in the specimen chamber was held constant at 10°C, and changes in relative humidity were induced by changing the water vapor pressure in the specimen chamber. Each image was 512 × 512 pixels in size.

To explore the influence of age, water : cement ratio, and temperature, drying shrinkages were induced by two large RH decrements: 90% ⇒ 50% RH, followed by a drop to 5% RH.

3. Results

The results are divided into two sections: 1) experiments designed to be compared to the results of Roper and 2) experiments to explore the influence of age, w/c and temperature.

3.1. Relationship to Roper

The first set of experiments was designed for direct comparison with Roper's results. Figs 1 and 2 show the deformation maps for the $w/c = 0.35$ and $w/c = 0.50$ cement pastes, respectively, for the specified RH values. The parts of both figures come in pairs, (a)-(b), (c)-(d), etc. where the first image in the pair is for compaction, and the second image in the pair is for rarefaction. As RH is reduced, the images record the development of deformations due to drying shrinkage.

To obtain a more quantitative view of these phenomena, Figs 3 and 4 show the distributions of deformations (in the form of histograms) for the maps shown in Figs 1 and 2, respectively. These are computed as described in Ref. [1]. These distributions are normalized to the same value, so that the central peak, the top of which is not shown in any of the distributions, is lowered if the width of the distribution is broadened. Table III contains the results of integrating the curves with respect to both number and magnitude of deformation shown in Figs 3 and 4. These values are the sum of all of the deformations and therefore represent the average or overall deformation across the field of view.

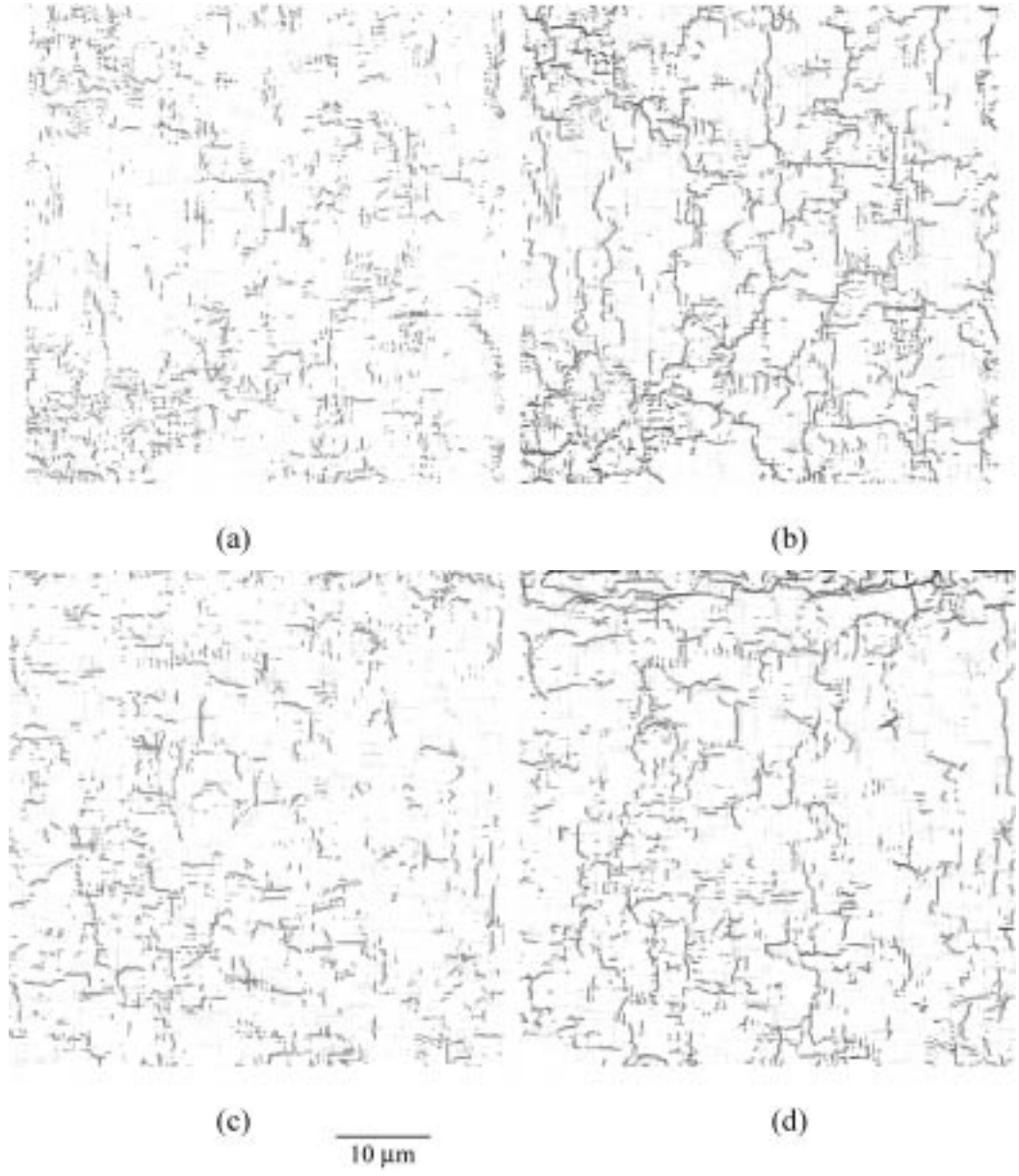

Figure 1 Deformation maps for a 7 day old sample of $w/c = 0.35$ cured at room temperature. In all maps, the field of view is approximately 96.8 μm × 96.8 μm. Darker colors indicate higher magnitude deformations. Compaction maps are shown for drying from 90% RH to (a) 80% RH; (c) 75% RH; (e) 55% RH; (g) 35% RH; and (i) 20% RH. Rarefaction maps are shown for drying from 90% RH to (b) 80% RH; (d) 75% RH; (f) 55% RH; (h) 35% RH; (j) 20% RH.

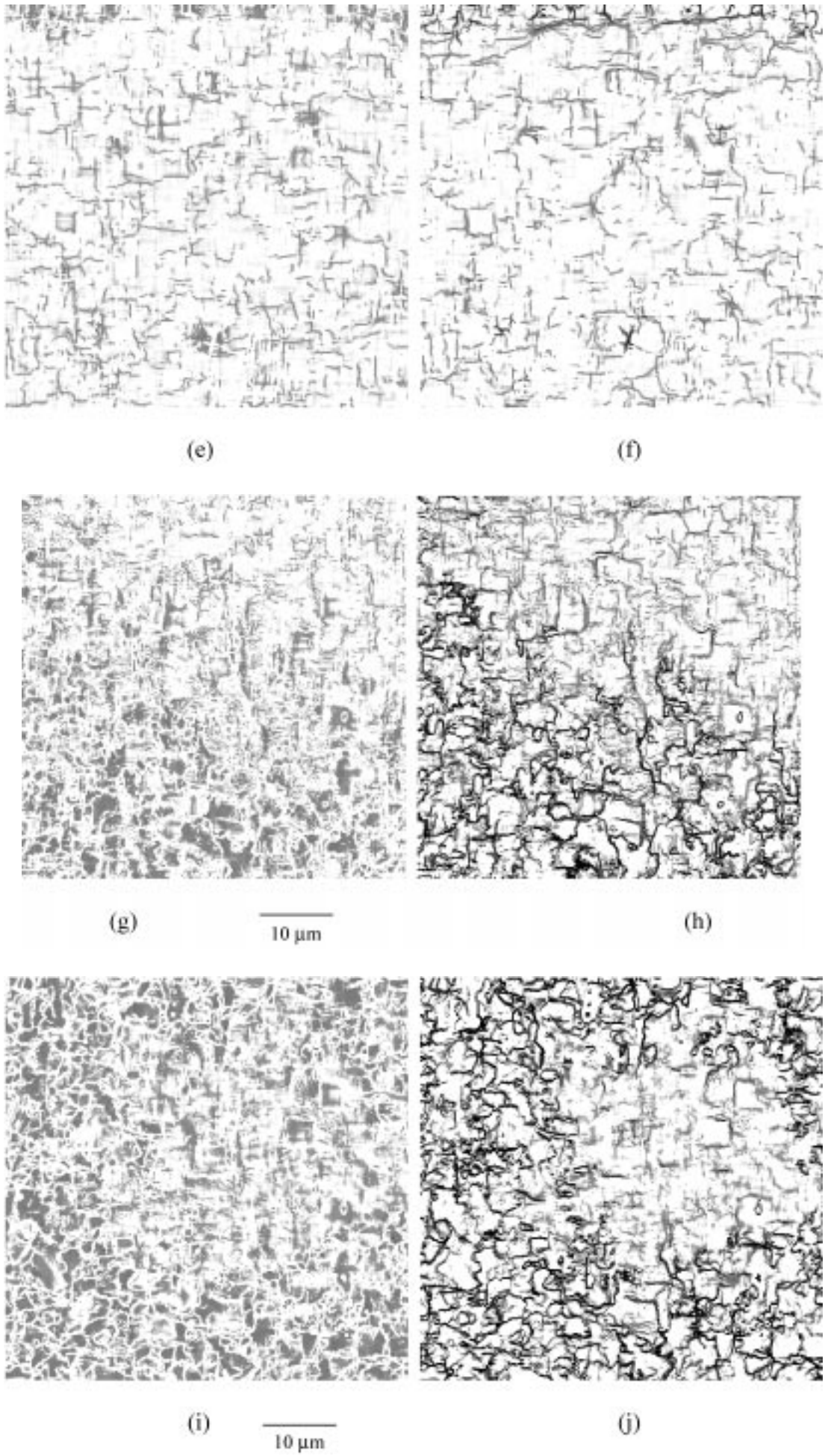

Figure 1 (*Continued*).

TABLE III Overall sample deformations computed by integrating under the deformation distribution curves

Relative Humidity	$w/c = 0.35$	$w/c = 0.50$
80%	0.01%	0.05%
75%	0.02%	0.11%
55%	0.08%	0.19%
35%	0.24%	0.32%
25%	—	0.51%
20%	0.29%	—

Fig. 1 contains typical deformation maps. Upon drying from 90% to 80% RH, the higher deformations, both compactions and rarefactions, are localized and to some extent linear. Table III gives an average shrinkage of 0.01% for this drying condition.

Upon drying to 75% RH, Fig. 1c and d show only slightly increased local deformations. The morphologies of both types of deformation fields remain linear, though they appear to have expanded slightly. It is interesting to note that while this relative humidity is below the first change in slope on Roper's curve [4], we observe no obvious change in mechanism based on the deformation maps. This will be commented on below. The distribution of deformations shown in Fig. 3 has become slightly wider, and the small peak at −10% deformation has increased slightly. Table III shows that the overall or average shrinkage has increased to 0.02%.

Fig. 1e and f show the deformation maps upon continued drying to 55% RH, near the lower end of the RH range where capillary stress is considered to be dominant. At this relative humidity, the first evidence of field-like compactions, accompanied by crack-like

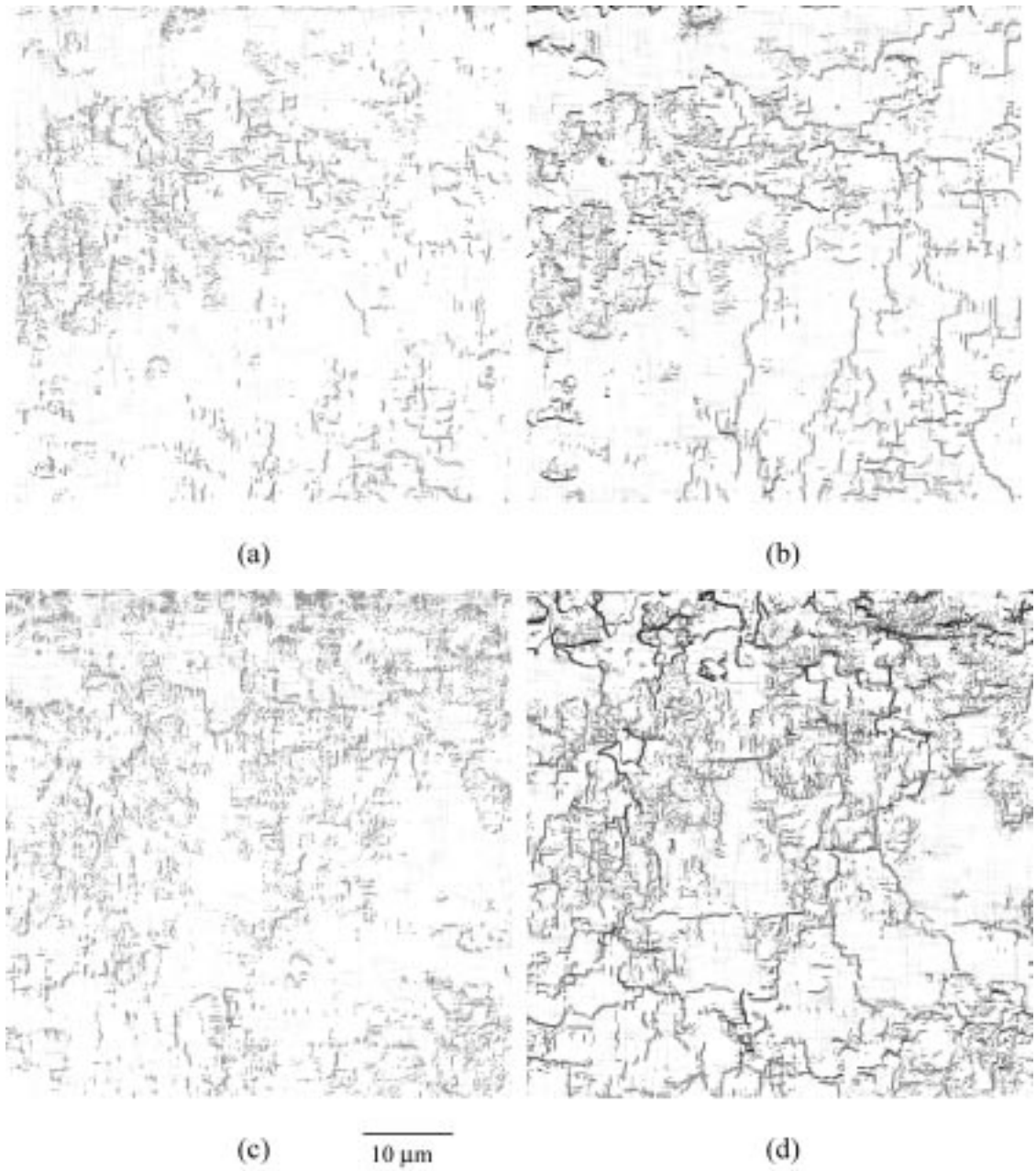

Figure 2 Deformation maps for a 7 day old sample of $w/c = 0.50$ cured at room temperature. In all maps, the field of view is approximately 96.8 μm × 96.8 μm. Darker colors indicate higher magnitude deformations. Compaction maps are shown for drying from 90% RH to (a) 80% RH; (c) 75% RH; (e) 55% RH; (g) 35% RH; and (i) 25% RH. Rarefaction maps are shown for drying from 90% RH to (b) 80% RH; (d) 75% RH; (f) 55% RH; (h) 35% RH; and (j) 25% RH.

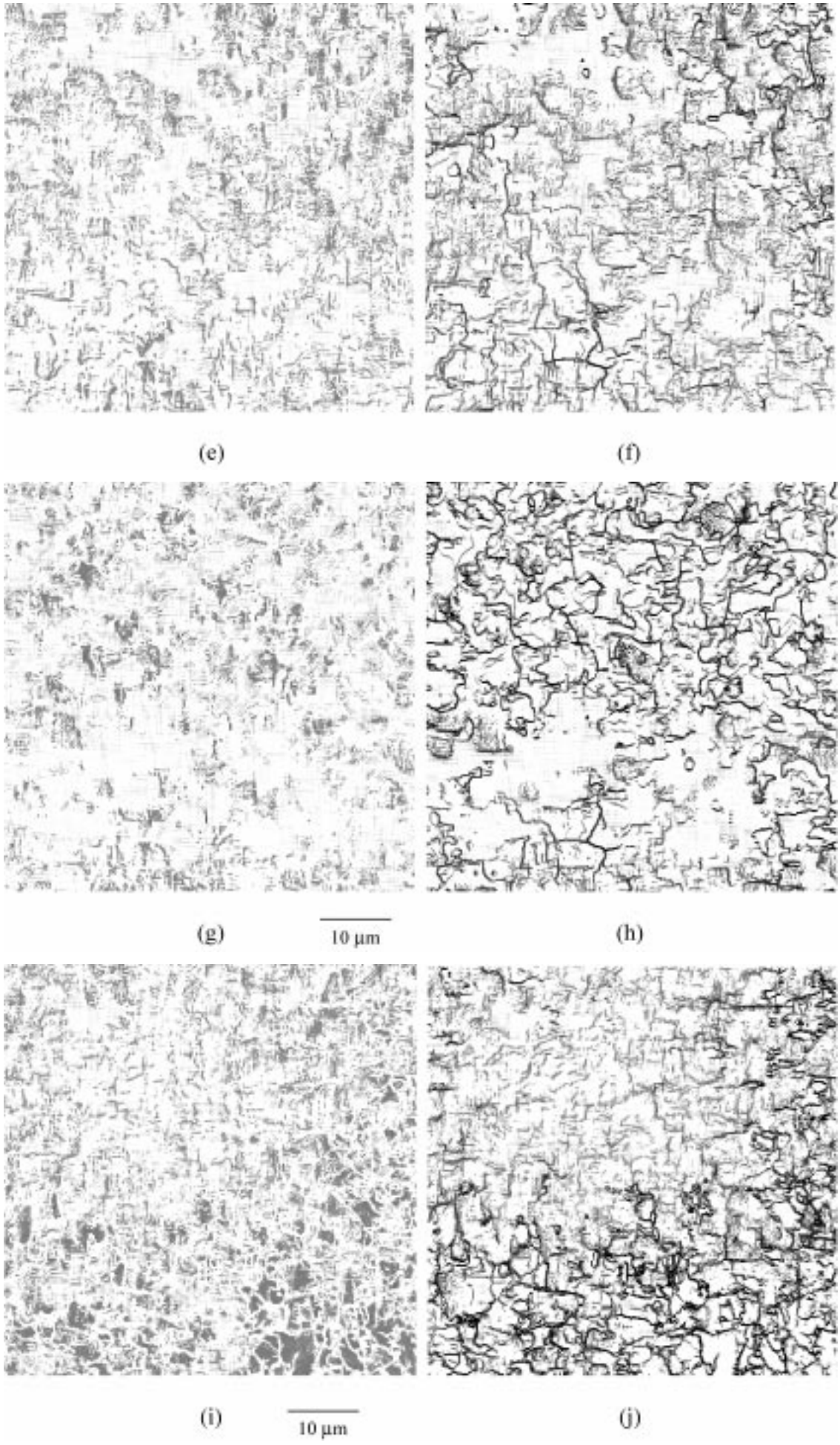

Figure 2 (*Continued*).

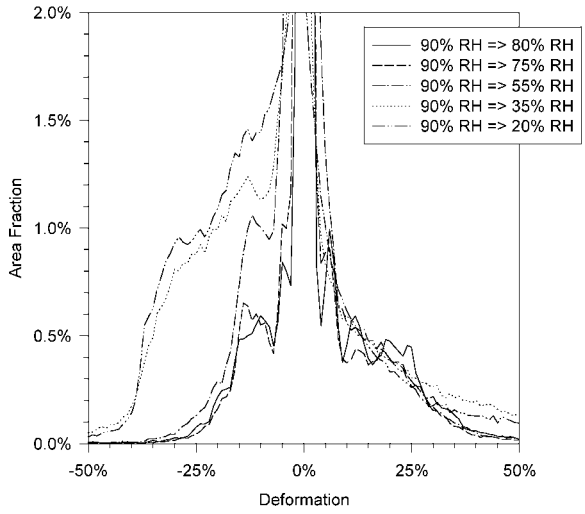

Figure 3 Deformation distributions for deformation maps shown in Fig. 2 for a 7 day old sample of $w/c = 0.35$ cement paste.

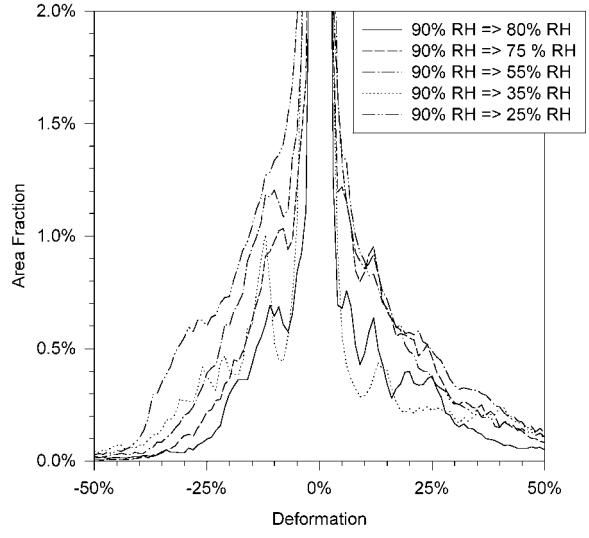

Figure 4 Deformation distributions for deformation maps shown in Fig. 3 for a 7 day old sample of $w/c = 0.50$ cement paste.

rarefactions, is observed. The appearance of these morphologies is accompanied by a significant increase in the overall shrinkage (0.08%), as shown in Table III. The compaction fields in these images are readily associated with the fields of C-S-H in the accompanying microstructural image (not shown). The deformation for this drying condition, 90% to 55% RH, shown in Fig. 3, provides some further important clues. The curve has again become slightly wider, consistent with the increased magnitude of deformation throughout the microstructure. The peak at −10% has increased significantly.

Continuing the drying process to 35% RH, as shown in Fig. 1g and h, results in compactions separated by linear areas of intense rarefactions. These deformation maps begin to be similar in morphology to those presented later for drying from 90% RH to 5% RH even though the overall strain level is lower. Fig. 1g and h show that significant areas of the microstructure have now deformed significantly. The distribution of deformations for the 35% maps suggest the onset of a second mechanism. As seen in Fig. 3, the distribution is significantly wider than any of the previous distributions, especially on the compaction (negative) side, and the overall shrinkage of the piece has increased to 0.24%, as shown in Table I. The peak at −10% deformation, tentatively associated with C-S-H, is still present, but it has been obscured by the broadening of the distribution.

Fig. 1i and j show the deformation maps due to drying to 20% RH. It is seen that the compactions and rarefactions continue to expand as drying continues, and the maps become very similar to those presented for drying from 90% to 5% RH as will be shown. Fig. 1i and j represent a point just below the third change in slope in Roper's curve [4] for $w/c = 0.35$, but no obvious mechanistic differences were noted between them and the 35% RH results. The overall distribution curve continues to increase in width, as shown in Fig. 3, now completely obscuring the peak at −10% deformation. Table III shows the overall deformation has now increased to 0.29%. The deformations for the $w/c = 0.5$ samples follow a similar path, but a higher magnitude is achieved.

Figs. 2 and 4 substantiate the general trends shown in Figs. 1 and 3. They are included because of their importance to the influence of *w*/*c*.

3.2. Influence of age, w/c, and temperature

Representative deformation maps and histograms that explore the influence of age, water : cement ratio, and

TABLE IV Overall drying shrinkage deformation upon drying from 90% to 50% and 90% to 5% RH (Bergstrom data [2, 3] and current data)

(1)	(2)	(3)	(4)	(5)	(6)	(7)	(8)
		Bergstrom Data [2, 3]		Bergstrom Methodology		Integration Under Curve	
w/c	Age (days)	90 ⇒ 50*	90 ⇒ 5*	90 ⇒ 50	90 ⇒ 5	90 ⇒ 50	90 ⇒ 5
0.3	4**	0.01%	0.20%	0.02%	0.24%	0.05%	0.30%
	14	0.00%	0.00%	0.02%	0.20%	0.01%	0.23%
	28	0.10%	0.10%	0.00%	0.10%	0.02%	0.11%
0.4	4**	0.05%	0.24%	0.06%	0.20%	0.09%	0.35%
	14	0.08%	—	0.04%	0.23%	0.04%	0.36%
	28	0.15%	0.18%	0.01%	0.08%	0.00%	0.14%
0.5	4**	0.30%	0.65%	0.15%	0.45%	0.24%	0.62%
	14	0.23%	0.39%	0.17%	0.21%	0.28%	0.32%
	28	0.15%	0.15%	0.09%	0.15%	0.13%	0.21%

*Bergstrom data measured from 80% ⇒ 40% RH and 80% ⇒ 5% RH

**Bergstrom data measured at 7 days of age

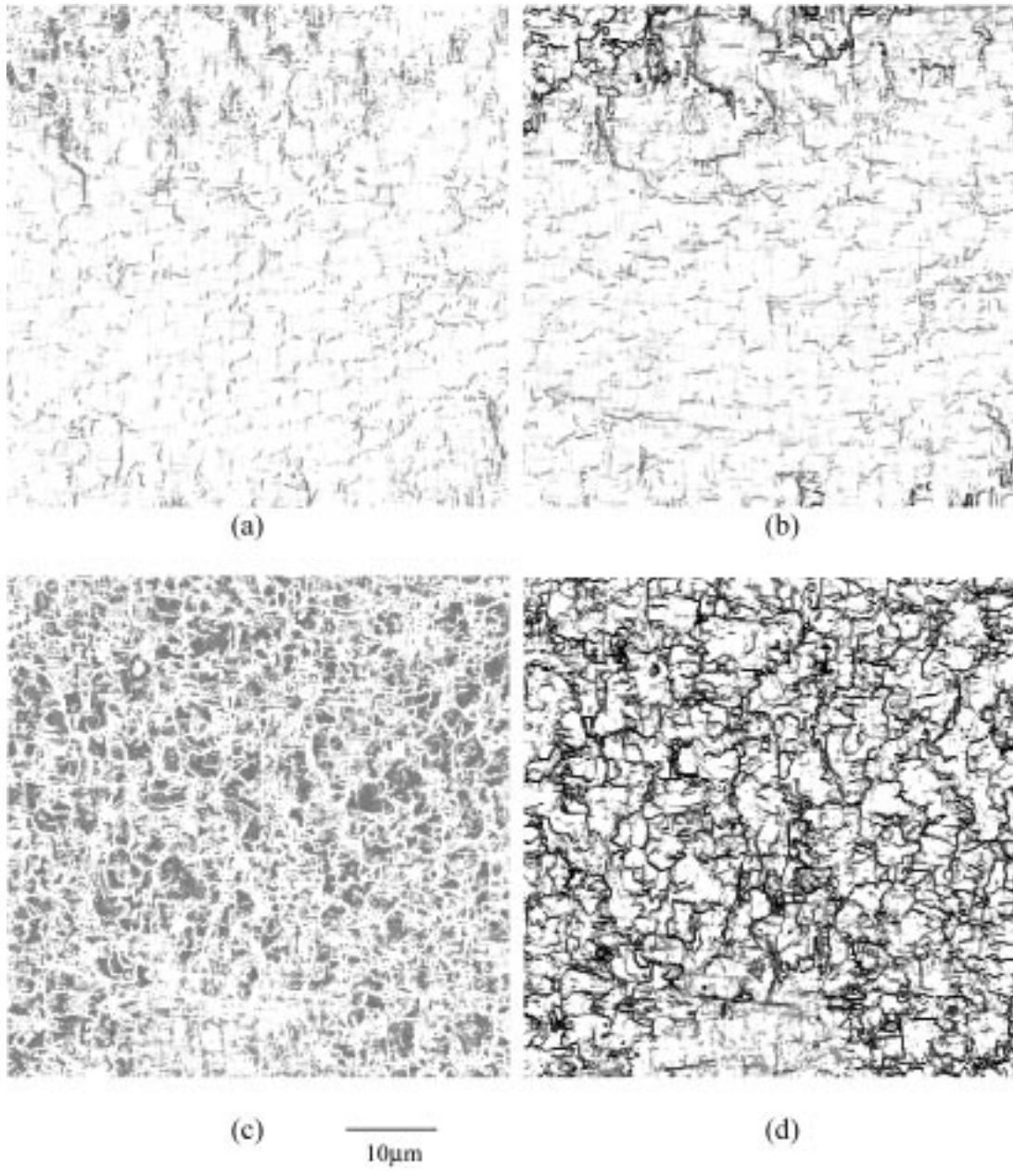

Figure 5 Deformation maps for a 4 day old sample of $w/c = 0.5$ cured at 20°C. In all maps, field of view is 96.8 μm $\times$ 96.8 μm. Darker colors indicate higher magnitude deformations. (a) Compactions for 90% $\Rightarrow$ 50% RH. (b) Rarefactions for 90% $\Rightarrow$ 50% RH. (c) Compactions for 90% $\Rightarrow$ 5% RH. (d) Rarefactions for 90% $\Rightarrow$ 5% RH.

curing temperature are shown in Figs 5–10. In these figures, parts (a) and (c) are compaction maps and part (b) and (d) are rarefaction maps, parts (a) and (b) are for the 90% RH to 50% RH drying regime, and parts (c) and (d) for the 90% RH to 5% RH drying regime. Table IV shows the results of various analyses for the age and water : cement ratio experiments. The third and fourth columns (labeled *Bergstrom Data*) show the data of Bergstrom [3]. The fifth and sixth columns (labeled *Bergstrom Methodology*) were compiled using Bergstrom's method for computing overall shrinkage strain on the samples studied in this paper. This method computes $\Delta l/l$ for several pairs of points, separated across the image, and averages the results. The deformation mapping technique used in this paper averages over the entire sample and uses the correct mathematical method of mapping displacements for large strains, and is therefore more accurate [5]. These numbers are given in the seventh and eighth columns (labeled *Integration Under Curve*) of Table IV. Broad trends of the results of this research are shown in Table V. Although

TABLE V Trends of micro-scale and macro-scale deformations as a function of increasing age, w/c, and temperature under two different drying conditions

Drying Condition	Variable Increasing	Magnitude of Micro-scale Deformations	Magnitude of Overall Deformation
90% RH	Age	Increase	Decrease
$\Downarrow$	w/c	Decrease	Increase
50% RH	Temperature	Decrease	???
90% RH	Age	Little Change	Decrease
$\Downarrow$	w/c	Little Change	Increase
5% RH	Temperature	Decrease	Decrease

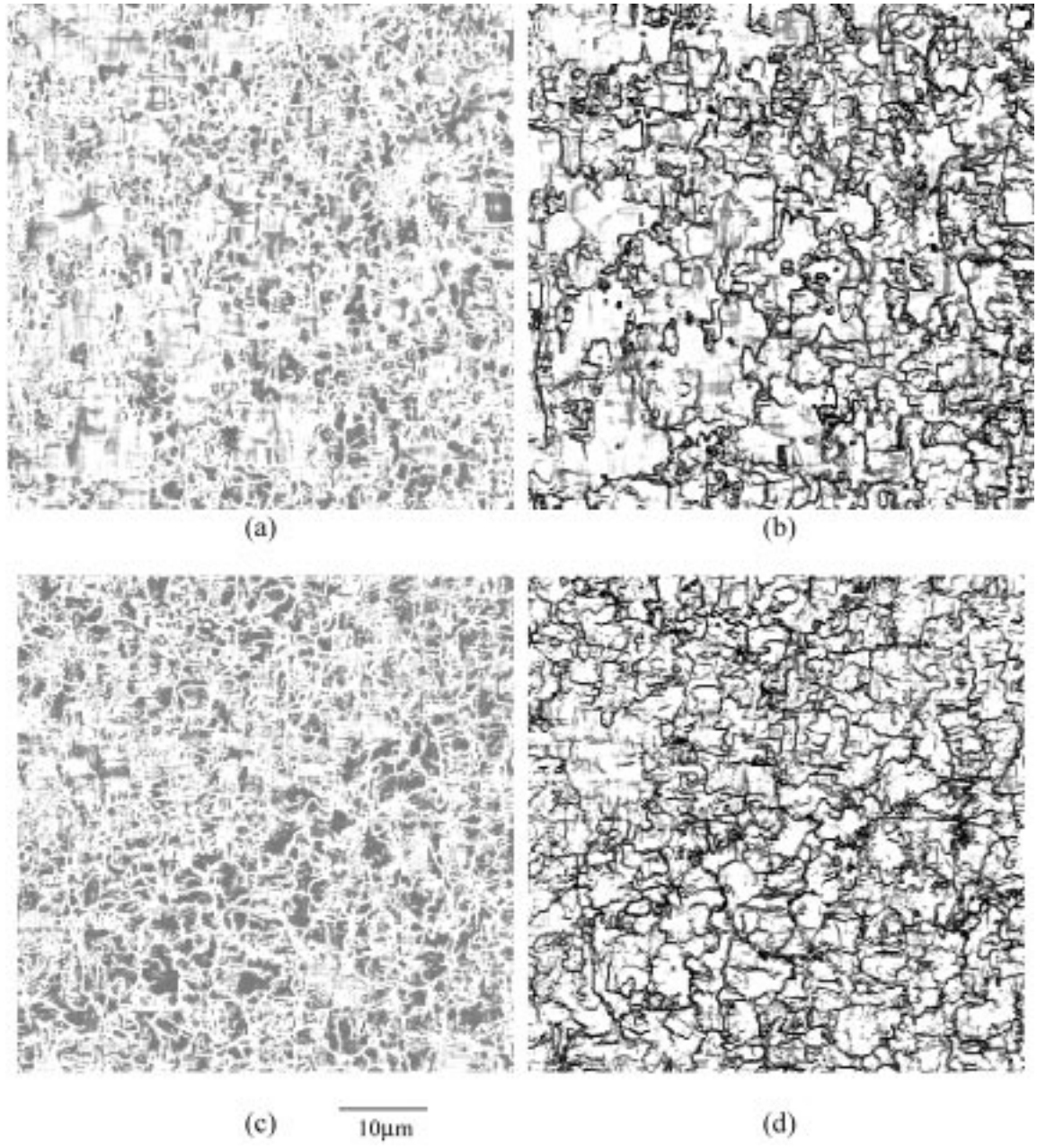

Figure 6 Deformation maps for a 28 day old sample of $w/c = 0.5$ cured at 20°C. In all maps, field of view is 96.8 μm × 96.8 μm. Darker colors indicate higher magnitude deformations. (a) Compactions for 90% ⇒ 50% RH. (b) Rarefactions for 90% ⇒ 50% RH. (c) Compactions for 90% ⇒ 5% RH. (d) Rarefactions for 90% ⇒ 5% RH.

the magnitudes from these different techniques are somewhat different, the trends are similar. Similar results for the influence of temperature experiments are shown in Table VI.

A large number of strain maps have been studied, including samples containing mineral admixtures [22] and samples damaged during freezing. Some trends are emerging that help interpret this new type of information.

TABLE VI Influence of temperature on overall drying shrinkage deformation upon drying from 90% to 50% and 90% to 5% RH. Each sample is 28 days old and has a $w/c = 0.3$

	Overall Shrinkage Deformation	
Curing Temperature	90% RH ⇒ 50% RH	90% RH ⇒ 5% RH
20°C	0.02%	0.11%
30°C	0.05%	0.07%
40°C	0.01%	0.04%

Referring first to the histograms, it has proven useful to divide them into two parts, 1) -6% to $+6\%$ and 2) $< -6\%$ and $> +6\%$. For pastes dried to 50% RH, the sum of the deformations in category 2 almost always total zero. In other words, even though the shapes of the histograms are different, the total compactions equal the total rarefactions. On the other hand, the total deformation in category 1 is not generally equal to zero, but is nearly equal to the integration under the entire histogram, i.e. the values in columns seven and eight in Table IV. This set of numbers will be compared to the measured shrinkage across the field of view.

Typically patterns of compactions are less well defined than rarefactions. At higher relative humidities, both have some resemblance to a microcracking

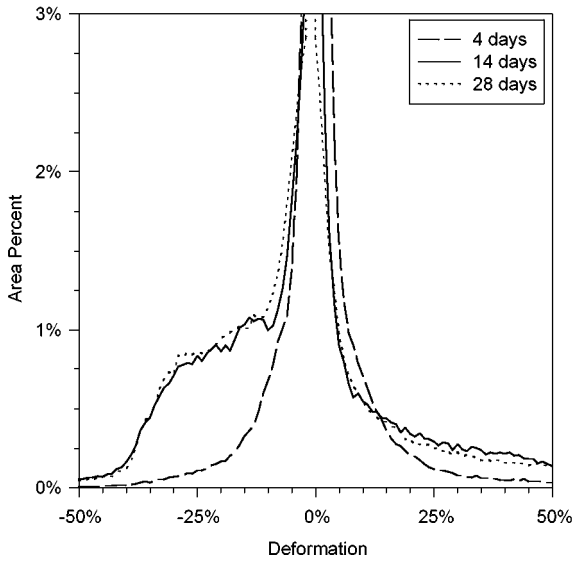

(a)

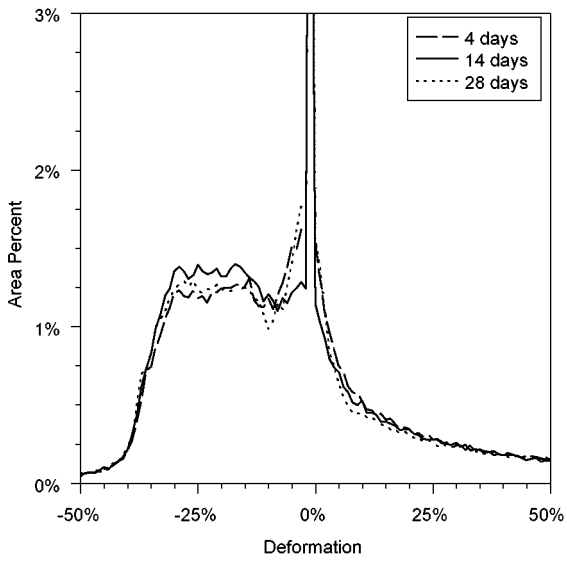

(b)

Figure 7 Deformation distributions for deformation maps shown in Figs 1–3 for a sample of $w/c = 0.5$ cured at 20°C at 4, 14, and 28 days of age for: (a) 90% ⇒ 50% RH, and (b) 90% ⇒ 5% RH.

pattern, but the lines are more discontinuous in the compaction map. Only a few percent of the deformations are greater than 15%, which may be noise. Almost all of the deformation is less than 6%. The histograms are fairly broad and are nearly symmetric.

As the relative humidity is lowered, the rarefactions become more intense, but they maintain the appearance of a network of cracks that become more interconnected. The compactions lose the appearance of lines and in many regions become fields. In all cases, where compaction patches form (as the RH is lowered), the histograms show broad shoulders at deformations greater than 6%. Furthermore pastes with smaller capillary porosity display larger shoulders at intermediate relative humidities (i.e. ∼50%). This is a general result.

Before starting the general discussion, a few points on possible sources of artifact are appropriate. Since the large deformations (>6%) at 50% RH have very consistent patterns, and since compactions nearly equal rarefactions, they can not be interpreted as either noise or as deformations that are associated directly with bulk shrinkage. The shoulder at 50% is probably deformation that results from processes other than volume change related to bulk shrinkage. Curling and crumpling of C-S-H during drying has been observed using transmission electron microscopy [23], which could be analyzed as large compactions of C-S-H and large rarefactions of a pore, or the edges of a pore. Another physical change that occurs at higher RH is the removal of water from the capillary pore system. Liquid water is a disappearing phase, and this could appear as a shrinking phase with very large deformation. If the pores are large, they are mainly empty at 90% RH, and no deformation will be observed at 50% RH. On the other hand, if they are small, water will be removed in this range.

4. Discussion

The value of the DMT depends on interpretation. Since the technique is new, this discussion will focus on some of the most consistent and pronounced trends and make comments in terms of possible mechanisms.

4.1. Bulk shrinkage

The most obvious observation is that bulk shrinkage is the result of competition between compactions and rarefactions. The rarefactions can have the appearance of cracks although no open cracks are observed. This observation may be relevant to the so-called drying creep [12], sometimes referred to as the Pickett effect. A common explanation for the greater than linear coupling of deformation under simultaneous load and drying is that the load prevents cracks which would otherwise form and causes a superimposed expansion. Lack of cracks increases the measured shrinkage. The cracks are hypothesized to come from stress due to gradients as water evaporates from the surface of thicker samples. The effect, therefore, depends on the size of the sample. If the cracks form in the absence of external stress, bulk shrinkage is less than intrinsic shrinkage. This may be mitigated by using very thin samples and very slow drying. The results of this study indicate that rarefactions result from shrinking and restraining phases at the micrometer scale, and moisture gradients at larger scales do not need to be invoked to produce crack-like rarefactions that could be altered by applied stress. This implies that the Picket effect is not necessarily dependent on size at the scales previously thought.

4.2. Comment on large deformation

As will be shown throughout this paper, Figs 3 and 4 (except for 35% RH in Fig. 4) represent several typical trends. Before examining these details, however, the observation of very large deformations require comment. At higher RH, compactions up to 15% are observed, and at lower RH, compactions of 40% are observed. Although the shoulder is less pronounced for rarefactions,

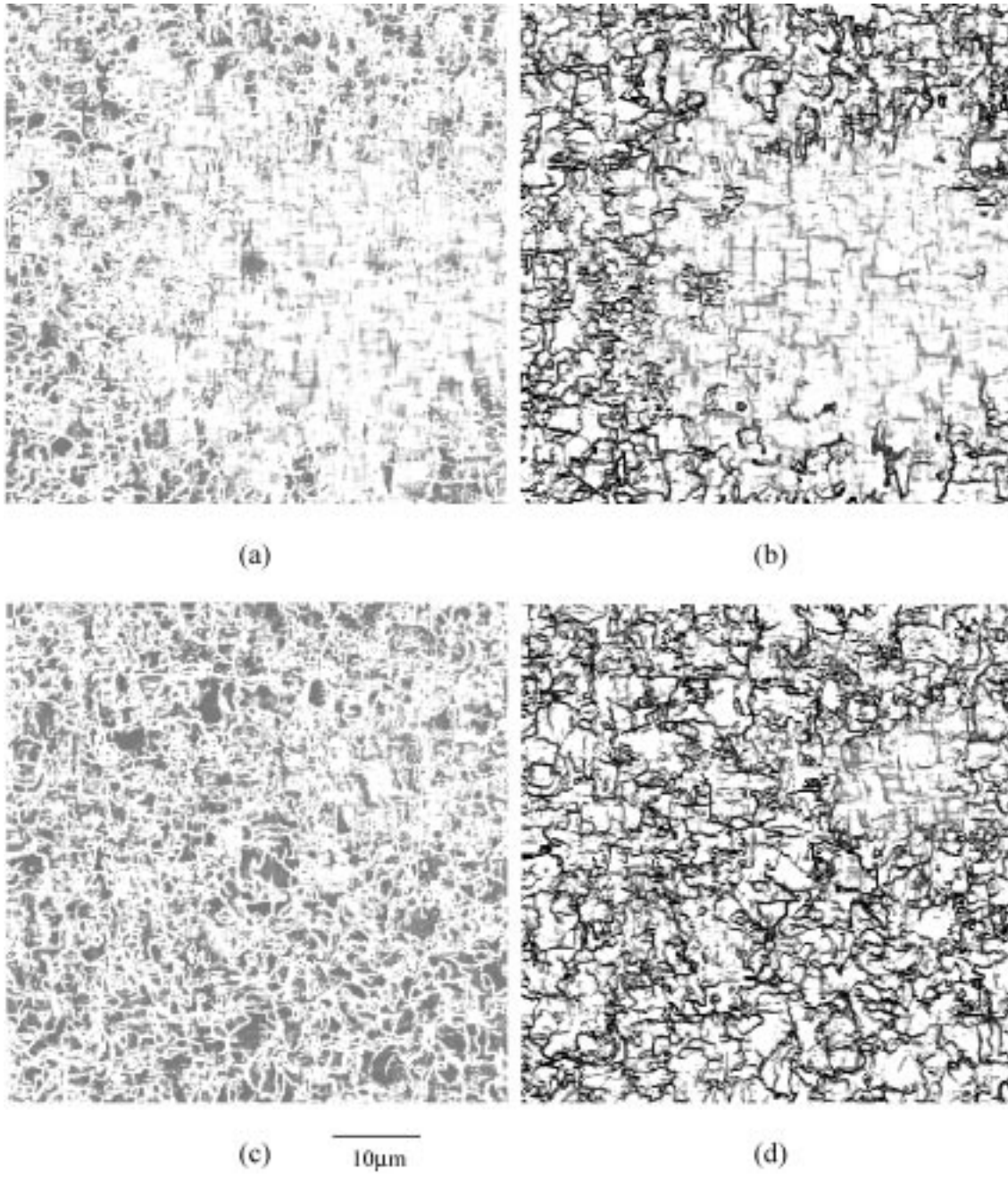

Figure 8 Deformation maps for a 4 day old sample of $w/c = 0.3$ cured at 20°C. In all maps, field of view is approximately 96.8 μm $\times$ 96.8 μm. Darker colors indicate higher magnitude deformations. (a) Compactions for 90% $\Rightarrow$ 50% RH. (b) Rarefactions for 90% $\Rightarrow$ 50% RH. (c) Compactions for 90% $\Rightarrow$ 5% RH. (d) Rarefactions for 90% $\Rightarrow$ 5% RH.

a significant number of pixels represent huge deformations, and a similar statement can be made. These large deformations can not be explained by capillary stresses from an emptying pore system.

Large deformations can be explained, however, by considering the structure of C-S-H to be precipitated tiny particles with radii of about 1.1 nm [24]. If this is the case, then at least some of the C-S-H network collapses on drying, a process which may be similar to the "constant rate period" observed for colloids, which can account for volume changes greater than an order of magnitude for colloids [23]. The constant rate period is a process where liquid is removed from a gel, and the capillary stress causes the solids to become more densely packed. Ideally, the pores do not empty, but for C-S-H, with a wide range of pore sizes, drying probably empties the larger pores. Thus, large deformations observed here supports the possibility that C-S-H is a colloidal material that collapses on drying [24].

At some point, the constant rate collapse ends, and the structure stiffens and stops collapsing. At this point, a meniscus is unstable, and on further drying, the remaining pores empty. As with colloids [23], further shrinkage is small (for colloids, this is the first falling rate period), and sometimes small expansion occurs. During this period, the colloid is weakened, and fracture occurs. Finally at the lowest relative humidity, the last few layers of water are removed, and Gibbs-Bangham shrinkage occurs.

These ideas do not differ greatly from the standard mechanisms outlined earlier. The main addition here is the possibility of very large local deformations

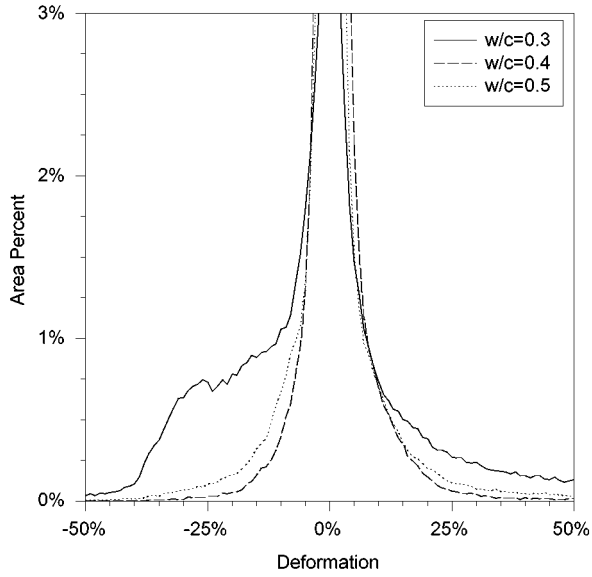

(a)

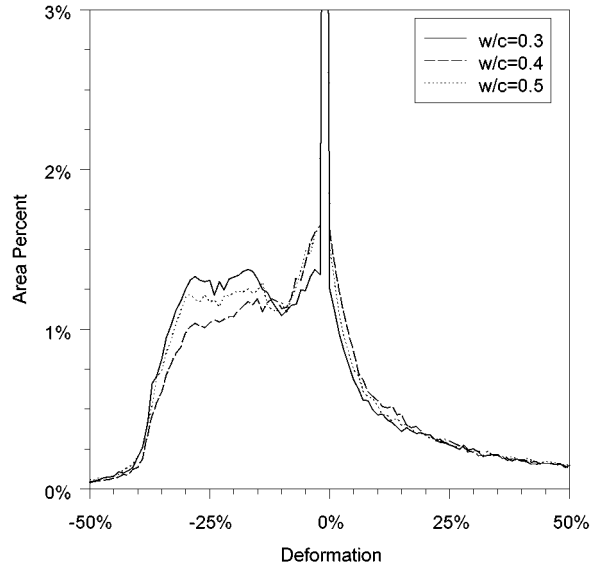

(b)

Figure 9 Deformation distributions for deformation maps shown in Figs 1, 6, and 7 for a 4 day old sample cured at 20°C at $w/c = 0.3$, 0.4, and 0.5 for: (a) 90% RH ⇒ 50% RH, and (b) 90% RH ⇒ 5% RH.

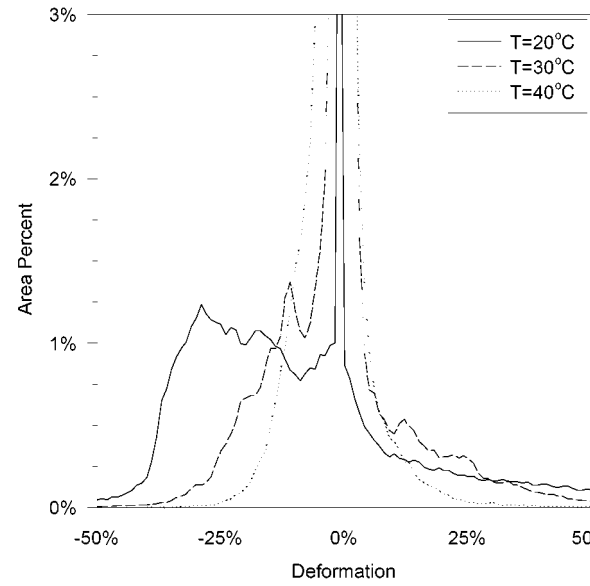

(a)

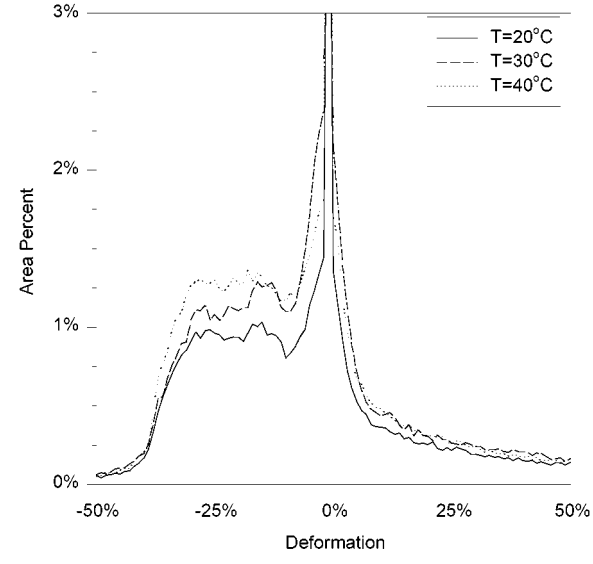

(b)

Figure 10 Deformation distributions for deformation maps shown in Figs 9–11 for samples of $w/c = 0.3$ cured at 20°C, 30°C, and 40°C at 28 days of age after drying for: (a) 90% ⇒ 50% RH, and (b) 90% ⇒ 5% RH.

analogous to the constant rate period in colloids. This possibility will be considered in the following discussion.

4.3. Drying in a stepwise fashion and relationship to mechanisms

As shown in Figs 3 and 4 (except for 35% in Fig. 4), a number of trends are established that will be discussed further in the next section. On drying to 80% RH, only a small amount of shrinkage occurs (as per Roper), but a relatively large amount of water is removed. Water is removed from pores larger than about 10 nm radius. Only a small percentage of the area of the micrograph exhibits large deformation, and both rarefactions and compactions are dispersed across regions that can be identified as C-S-H. Further drying causes this structure to further collapse, and the larger pores to empty. A relatively small amount of water is lost, but a large amount of shrinkage occurs. This is analogous in part to the constant rate period observed in colloidal systems [23] and in part to the more accepted idea of capillary stress causing shrinkage as pores are emptied. This collapse is largely responsible for irreversible shrinkage. At 55% RH all of the pores with radius greater than about 2 nm have emptied, although at this point the concept of capillary stress is not valid because the meniscus is unstable. Drying to 35% RH greatly increases the area percentage of the large deformations, and the large deformations become much more localized. Compactions cluster into regions, and rarefactions appear as tangled lines. The compactions are always surrounded by rarefactions. The rarefactions

appear crack-like. We propose that these patterns form during drying that is analogous to the first falling rate period in colloids [23] when the network is subjected to large stress due to gradients, and attractive forces are reduced as capillary stress disappears. The cracks allow C-S-H to relax, forming compaction regions.

When the deformations maps are printed on transparencies and overlayed on a micrograph, it is clear that both compactions and rarefactions are distributed across one grain or contiguous region of C-S-H. As drying occurs, pixels representing large deformation become more localized, forming particles (compactions) and linear regions (rarefactions). As the RH is lowered, the compactions group together. The C-S-H collapses to its densest structure, and crack-like formations crisscross the region. As will be shown, the more abundant the C-S-H within a field of view (i.e. lower w/c) and/or the stiffer the matrix (at least for the ages of sample discussed here), the higher is the RH at which the localization process results in particles. At the ages of concern in this paper, essentially no visible changes occur in the micrographs during drying. However, as can be seen at much earlier ages, Fig. 11, comparison of a wet and dry sample shows rarefactions with a crack-like pattern and compactions that are easily visualized. We suggest that DMT is allowing this to be seen in older samples.

Further drying to 20% RH produces little further bulk shrinkage as shown by Roper. Fine pores empty, but adsorbed water is not removed. C-S-H fractures and relaxes. As shown in the rest of the Figs 5–10, the final stage, from 20% RH down, exhibits large deformations for many pixels. The adsorbed water is removed, and relatively large bulk shrinkage is observed. This is Gibbs-Bangham shrinkage, and because of the extensive area with large deformations, it must involve all of the C-S-H, whereas deformation at higher RH's seems to involve only some of the C-S-H. This would be consistent with only low density C-S-H collapsing [24] at the higher RH's, and all of C-S-H shrinking at the lower RH's.

Figs 3 and 4 show a more pronounced compaction shoulder at the lower w/c. The stiffer sample has more larger deformations at 35% RH. More fracture and relaxation occur in a stiffer matrix. This at first surprising trend has been observed in all of our samples.

Some support for fracture being associated with high deformation comes by analogy to colloids. After the constant rate period, the structure stiffens and water begins to empty from the pore system. During this period, the network can actually expand somewhat [23]. Differential stresses within the gel network makes this the most likely time of fracture. Previously unexplained data published in ref. [4], one figure of which is included here, Fig. 12, can now be reconciled. During drying, tiny specimens exhibit continuously increasing shrinkage with decreasing RH, however, during specific relative humidity drops from 40–20% RH for the top line in Fig. 12, shrinkage is greatly reduced, is large, irreversible shrinkage is small. LD C-S-H is shrinking, but also the framework is highly restrained, resulting in fracture before complete collapse can occur.

The interpretation here is that when the shoulder exists, the C-S-H is compacting heterogeneously as a result of drying, causing curling, crumpling and fracture of the C-S-H as has been seen in ref. [28]. This occurs at intermediate RH's when the matrix is heavily

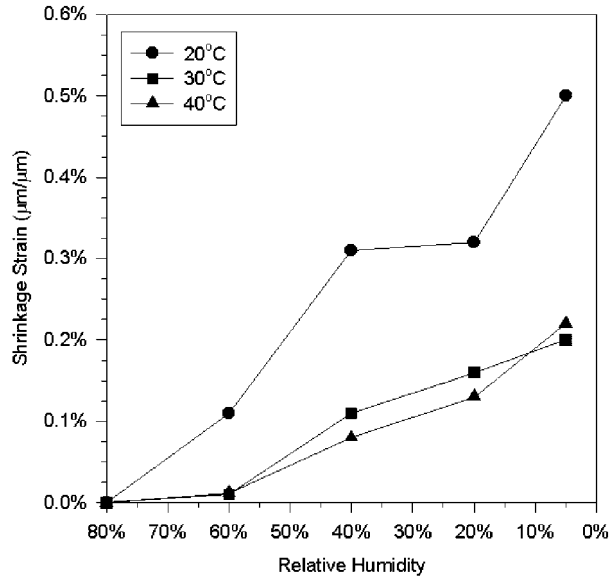

Figure 12 Shrinkage across a micrograph (100 μm) at various curing temperatures for 28-day-old cement paste of $w/c = 0.5$. (●), 20°C; (■), 30°C; (▲), 40°C [30].

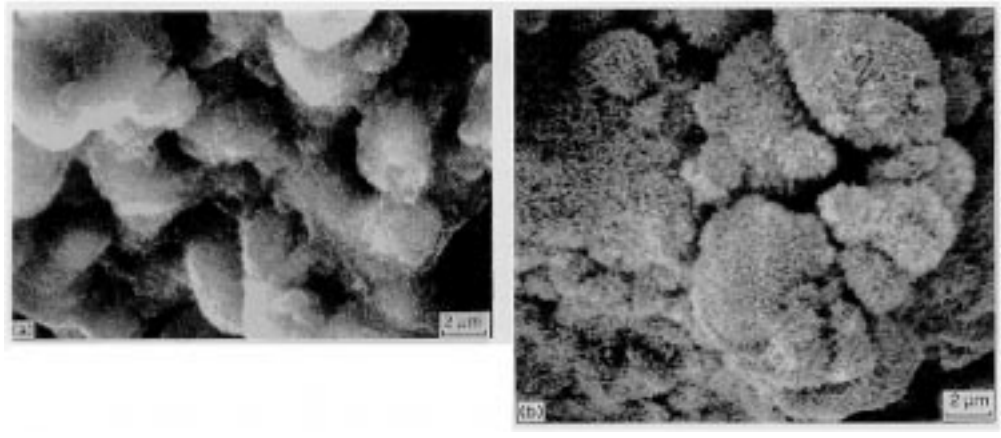

Figure 11 Tricalcium silicate hydrated for 16 hrs. (a) 90% RH, observed in ESEM and (b) vacuum dried, observed in SEM [29].

restrained and/or when evaporation is highly asymmetric, i.e. from one surface. We are treating the C-S-H as a colloid and, therefore, it dries like a colloid. In colloids, cracking is most likely to occur at the critical point as pores begin to empty [23]. C-S-H probably does not technically have a critical point because the larger pores have already emptied, but when the smallest pores start to empty, fracture becomes likely. This point in C-S-H occurs between about 40–60% RH, the higher value for more restrained systems. In other words, differential shrinkage, enhanced by the presence of restraint, enhances the likelihood of fracture.

The width of the central peak around 0% deformation is also of interest. Higher water : cement ratio and younger age results in broader peaks at 3% deformation. It should be noted by the scale of the ordinate on the figures that most pixels still show little or no deformation. However, these conditions have a greater percentage of deforming pixels in the $-6 \leq \times \leq 6\%$. It has been shown in other research that this range of deformation can be linked mathematically to bulk shrinkage, and the results here are consistent with this observation.

There is not much to distinguish differences in the histograms between different water : cement ratios and ages upon drying to 5%. As shown in Fig. 3, most of the shoulder is formed by 35% RH (this curve in Fig. 4 seems to not follow any of the trends thus showing behavior similar to the first falling rate of colloids when water starts evaporating from the pore system, and both fracture and overall expansion can be observed. Furthermore, the stiffer the sample, the higher the RH where fracture occurs, and the higher the RH where the shoulder becomes pronounced. These trends are summarized in Tables V and VII.

4.4. Influence of age and water : cement ratio shrinkage

Both age and water : cement ratio influence the size and tortuosity of the capillary pores and the amount and spatial distribution of hydration products including C-S-H, and both influence modulus as outlined in Table V. Study of both the deformation maps and the histograms supports the trends already outlined. Stiffer samples result in larger shoulders at 50% RH. This collapsing structure could also be a mechanism behind irreversible shrinkage. The collapsed precipitate does not return to its more open structure upon rewetting. This has some similarities to the mechanism proposed by Feldman and Sereda ([21], reported in [25]) who suggested that drying caused bonding between layers of C-S-H, but here the water is being removed from pores at relatively high humidities, and not from interlayers at lower humidities.

Irreversible shrinkage and total porosity [26] are related. Irreversible shrinkage can also be correlated with the abundance of pores in the 3–10 μm range [27]. These fine pores, as measured by nitrogen, are directly related to the quantities of low density C-S-H in the sample. Thus, shrinkage due to drying to 50% RH may be related to shrinkage of the low density C-S-H. Also a qualitative inverse correlation can be made between the presence of compaction shoulder at 50% RH and irreversible shrinkage. If the shoulder discussed in this paper), which is the RH where the second discontinuity in Roper's curves occurs. However, at 50% RH a large fraction of the microstructure has deformed. All of the C-S-H must be shrinking by Gibbs-Bangham mechanism at this point.

TABLE VII Relationships between modules and porosity, and age, initial w/c and curing temperatures of cement paste

		Effects of Increasing:		
Phase	Characteristic	Age	w/c	Curing T
Paste	Modulus	Increase	Decrease	Increase
Porosity	Amount	Decrease	Increase	Increase
	Average Size	Decrease	Increase	Increase

4.5. Influence of temperature

Since the influence of temperature on microstructure is less well understood, this section analyzes the microstructure in terms of the hypothesis. These samples are 28 days old, and the percent reacted at each temperature is roughly the same at 75% [27].

As shown in Fig. 10, at 50% RH the compaction shoulder is inversely related to temperature. A hint about the influence of temperature in terms of the mechanisms described here is seen in Fig. 12 from ref. [4], showing that there is little shrinkage at the higher RH's. The network structure of C-S-H has collapsed prior to drying. Furthermore, at higher temperatures, the width of the peak in Fig. 10 representing small deformation indicates that much of the microstructure is not changing. Bulk shrinkage at higher temperature, Table VII, is less than at lower temperature.

At 5% RH, a greater number of pixels deform in the shoulder at higher temperatures which may be the result of a little more hydration product.

5. Summary

The new technique of mapping deformation in the microstructure has been applied to shrinking cement paste. An attempt has been made to interpret the results in terms of mechanisms of shrinkage at different relative humidities. The following are hypotheses related to shrinkage.

- Bulk shrinkage is the result of competing expanding and shrinking parts of the microstructure.
- At 90% RH, the capillaries are essentially emptied.
- Down to 40% RH, the capillaries get bigger as the colloidal C-S-H collapses, a process partially analogous to the constant rate period observed for other colloids. During this stage, many of the pores within C-S-H do not empty as water evaporates from the surface of the compacting C-S-H precipitates. Very large and mostly irreversible shrinkage occurs during this stage. This is a process driven by capillary tension. It is a mechanism for shrinkage that differs from elastic shrinkage due simply

to capillary tension on pore walls. The collapse of the structure of C-S-H gel can account for very large deformations.

- From 40–20% RH, the porosity within the C-S-H empties. A meniscus is not stable. Greatly reduced shrinkage occurs for the associated water loss.
- In the middle range of RH's, the C-S-H can fracture and deform causing very large local rarefactions that have a crack-like pattern, and regions of compaction.
- At the higher RH's, only part of the C-S-H appears to shrink. This may be a low density C-S-H. At low RH, all the C-S-H appears to shrink.
- Below 20% RH the surface water is removed from the colloid C-S-H particles. Relatively large shrinkage occurs.

Although these are simply hypotheses, the results of DMT can be used to help further our understanding of deformation. Deformation maps represent a new kind of microstructure.

Acknowledgements

The authors gratefully acknowledge the financial support provided by the U.S. Department of Energy (Award CE-FG02-91ER45460). C.M.N wishes to thank the Department of Defense for funding via a National Defense Science and Engineering Graduate Fellowship.

References

1. C. M. NEUBAUER, E. J. GARBOCZI and H. M. JENNINGS, *J. Mater. Sci.*, submitted.
2. F. H. WITTMANN, in "Fundamental Research on Creep and Shrinkage of Concrete," edited by F. H. Wittmann (Martinus Nijhoff Publishers, Boston, 1962) p. 129.
3. T. B. BERGSTROM, PhD Thesis, Northwestern University, 1993.
4. C. M. NEUBAUER, T. B. BERGSTROM, K. SUJATA, Y. XI, E. J. GARBOCZI and H. M. JENNINGS, *J. Mater. Sci.* **32** (1997) 6415.
5. Y. XI, T. B. BERGSTROM and H. M. JENNINGS, *Comp. Mater. Sci.* **2** (1994) 249.
6. Y. XI and H. M. JENNINGS, in "Materials Science of Concrete III," edited by J. P. Skalny (American Ceramic Society, Westerville, OH, 1992) p. 37.
7. H. ROPER, *Hwy. Bd. Spec. Rpt.* **90** (1966) 74.
8. Z. P. BAZANT, *Cem. Concr. Res.* **2** (1972) 1.
9. R. A. HELMUTH and D. H. TURK, *J. PCA Res. Dev. Labs.* **9** (1967) 8.
10. F. O. SLATE and B. L. MEYERS, in International Conference on Structure, Solid Mechanics, and Engineering Design in Civil Engineering Materials, 1969, p. 769.
11. E. G. SWENSON and P. J. SEREDA, *J. Appl. Chem.* **7** (1967) 198.
12. S. MINDESS and J. F. YOUNG, "Concrete" (Prentice-Hall, Inc., Englewood Cliffs, NJ, 1981).
13. H. F. W. TAYLOR, "Cement Chemistry" (Academic Press, London, 1990).
14. Y. XI and H. M. JENNINGS, in "Materials Science of Concrete III," edited by J. P. Skalny (American Ceramic Society, Westerville, OH, 1992) p. 37.
15. C. F. FERRARIS and F. H. WITTMANN, *Cem. Concr. Res.* **17** (1987) 453.
16. W. HANSEN, *J. Am. Ceram. Soc.* **70** (1987) 323.
17. J. A. ALMUDAIHEEM, *J. King Saud Univ., Eng. Sci.* **1** (1991) 69.
18. T. C. POWERS, in "International Conference on the Structure of Concrete" (Cement and Concrete Association, London, 1968) p. 319.
19. *Idem.*, *RILEM Bull. (Paris)* **33** (1966) 381.
20. D. J. C. YATES, *Proc. Roy. Soc. London A 224*, (1954) 526.
21. R. F. FELDMAN and P. J. SEREDA, *Eng. J.* **53** (1970) 53.
22. R. A. OLSON, PhD Thesis, Northwestern University, 1998.
23. C. J. BRINKER and G. W. SCHERER, "Sol-Gel Science: The Physics and Chemistry of Sol-Gel Processing" (Academic Press, San Diego, CA, 1990).
24. H. M. JENNINGS, *Cem. Con. Res.* **30** (2000) 101.
25. V. S. RAMACHANDRUN, R. F. FELDMAN and J. J. BEAUDOIN, "Concrete Science" (Heyden, London, 1981).
26. G. VERBECK and R. A. HELMUTH, in Proceedings of the Fifth InterSymposium of the Chemistry of Cement, Tokyo, 1968 Vol. III, p. 1.
27. M. C. GARCI, PhD Thesis, Northwestern University, 1999.
28. H. M. JENNINGS and P. L. PRATT, *J. Mat. Sci.* **15** (1980) 250.
29. T. B. BERGSTROM and H. M. JENNINGS, *J. Mater. Sci. Ltrs.* **11** (1992) 1620.
30. C. M. NEUBAUER, T. B. BERGSTROM, K. SUJATA, Y. XI, E. J. GARBOCZI and H. M. JENNINGS, *J. Mater. Sci.* **32** (1997) 6415.

Received 14 July 1998
and accepted 16 February 2000